Bistable emergence of oscillations in growing *Bacillus subtilis* biofilms

Rosa Martinez-Corral[a], Jintao Liu[b,c], Gürol M. Süel[d,e,f], and Jordi Garcia-Ojalvo[a,1]

[a]Department of Experimental and Health Sciences, Universitat Pompeu Fabra, 08003 Barcelona, Spain; [b]Center for Infectious Diseases Research, School of Medicine, Tsinghua University, Beijing 100084, China; [c]Tsinghua–Peking Center for Life Sciences, Tsinghua University, Beijing 100084, China; [d]Division of Biological Sciences, University of California, San Diego, La Jolla, CA 92093; [e]San Diego Center for Systems Biology, University of California, San Diego, La Jolla, CA 92093; and [f]Center for Microbiome Innovation, University of California, San Diego, La Jolla, CA 92093

Edited by Alan Hastings, University of California, Davis, CA, and approved July 23, 2018 (received for review March 22, 2018)

Biofilm communities of *Bacillus subtilis* bacteria have recently been shown to exhibit collective growth-rate oscillations mediated by electrochemical signaling to cope with nutrient starvation. These oscillations emerge once the colony reaches a large enough number of cells. However, it remains unclear whether the amplitude of the oscillations, and thus their effectiveness, builds up over time gradually or if they can emerge instantly with a nonzero amplitude. Here we address this question by combining microfluidics-based time-lapse microscopy experiments with a minimal theoretical description of the system in the form of a delay-differential equation model. Analytical and numerical methods reveal that oscillations arise through a subcritical Hopf bifurcation, which enables instant high-amplitude oscillations. Consequently, the model predicts a bistable regime where an oscillating and a nonoscillating attractor coexist in phase space. We experimentally validate this prediction by showing that oscillations can be triggered by perturbing the media conditions, provided the biofilm size lies within an appropriate range. The model also predicts that the minimum size at which oscillations start decreases with stress, a fact that we also verify experimentally. Taken together, our results show that collective oscillations in cell populations can emerge suddenly with nonzero amplitude via a discontinuous transition.

biological oscillations | delay-induced oscillations | subcritical Hopf bifurcation | delayed negative feedback | biofilm growth

One of the main defining features of collective self-organization in coupled dynamical systems is the requirement of a minimum system size (1). According to that scenario, the number of coupled elements behaves as a control parameter that has to exceed a certain threshold for collective behavior to arise (2). Evidence of biological processes requiring a critical cell density has been reported for instance in myoblast fusion (3), yeast glycolysis (4), amoebae aggregation initiation (5), and immune cell homeostasis (6), among others. The phenomenon also underlies the most commonly studied means of cell–cell communication in bacteria, namely quorum sensing (7–9). In fact, the emergence of synchronized oscillations due to coupling in general systems of interacting elements has been termed dynamical quorum sensing (10, 11), due to its conceptual links with bacterial communication.

In the studies of dynamical quorum sensing carried out so far, coupling usually connects all elements of the system in an all-to-all manner (global coupling), so that the interaction between one cell and the rest can be described by a mean-field approximation (5). Such a global-coupling approximation may not be valid, however, when the population is structured in space. This is the case, in particular, when communication between cells is not mediated by a rapidly diffusive signal, but by a pulse-coupling mechanism through which the cells become activated by their neighbors in a "bucket-brigade" manner. This happens for instance in neurons, which are coupled via chemical synapses, and, as we have reported recently, in bacterial biofilms (12), where the cells signal their immediate neighbors via potassium ions released by bacterial ion channels (13). In this latter case, electrical signaling enables bacteria in the interior of the biofilm (which are subject to severe limitation in their only nitrogen source, glutamate) to transmit their stress state to the cells in the periphery (Fig. 1*A*). Peripheral cells subsequently stop growing and allow glutamate to enter the biofilm, thereby releasing the stress in the interior (12). This constitutes a spatially distributed negative feedback, which acts with a non-negligible delay due to the relatively slow propagation of the stressor.

Delayed negative feedback is well known to induce oscillations (or even more complex aperiodic dynamical phenomena), in particular in biological systems such as gene regulatory networks (14–17), physiological control systems (18, 19), neuronal populations (20), and ecological communities (21). In *Bacillus subtilis* biofilms, the above-described delayed negative feedback leads to oscillations in growth and stress levels (12). This is shown in Fig. 1*B*, which depicts a biofilm growing under constant conditions in a microfluidic system (Fig. 1*A*) (12). In the filmstrip, the blue color represents light emitted by the fluorescent cationic dye Thioflavin T (ThT), which acts as a Nernstian voltage indicator that reports on the cellular membrane potential (cells light up when hyperpolarized) (13, 22). Hyperpolarization results from intracellular potassium release, which is in turn caused by stress (13). Thus, ThT is a reporter of cellular stress, and the ThT oscillations portrayed in Fig. 1*B* can therefore be considered periodic modulations in stress.

Significance

Cell communities can become resilient to stress by undergoing collective growth oscillations, which provide periodic stress relief and are collective in the sense that they arise only for large enough numbers of cells. Collective oscillatory phenomena usually emerge continuously as the system size increases, with oscillations starting with small amplitude and slowly growing as the cells proliferate. This behavior, however, is not appropriate in situations in which the population needs to implement a full-sized response quickly. Our combined theoretical and experimental study shows that collective oscillations in bacterial biofilm communities emerge via a discontinuous transition as their size increases. This behavior may provide an evolutionary advantage to cell communities, by allowing them to quickly alter qualitatively their dynamics in response to variations in external conditions such as stress.

Author contributions: R.M.-C., G.M.S., and J.G.-O. designed research; R.M.-C. and J.L. performed research; R.M.-C. and J.L. analyzed data; and R.M.-C. and J.G.-O. wrote the paper.

The authors declare no conflict of interest.

This article is a PNAS Direct Submission.

[1]To whom correspondence should be addressed. Email: jordi.g.ojalvo@upf.edu.

Published online August 20, 2018.

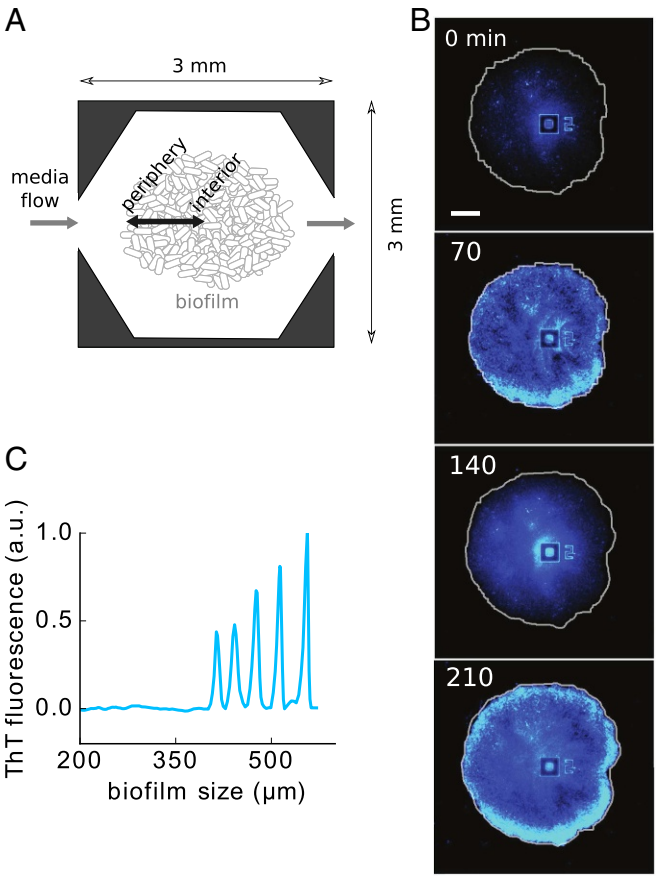

Fig. 1. Emerging oscillations in *B. subtilis* biofilms. (*A*) Scheme of the microfluidic device used to grow biofilms. (*B*) Filmstrip showing oscillations in stress reported by the membrane potential marker ThT. (Scale bar: 100 μm.) (*C*) ThT signal as the biofilm grows in size (radius), showing that the oscillations start only after a critical size is reached.

The oscillations described above exhibit two distinct characteristics. First, they appear only after the biofilm has reached a minimum size (12). This can be observed in Fig. 1*C*, which shows the ThT signal as a function of biofilm size (corresponding roughly to a time series, since system size increases monotonically with time). Second, as also shown in Fig. 1*C*, oscillations start with nonzero amplitude. Here we propose a basic explanation of these two facts in terms of a minimal delay-differential equation (DDE) model, in which the delay is considered explicitly. The minimal character of the model allows us to identify the essential features of the system that give rise to its nontrivial behavior. Specifically, our results show that delayed stress dynamics are sufficient to explain the experimentally observed discontinuous emergence of biofilm oscillations at a critical size.

The model makes two testable predictions. First, the discontinuous transition to oscillations takes the form of a subcritical Hopf bifurcation that entails the existence of a bistable region, where a stable state of steady growth coexists with the oscillatory regime described above. Second, the critical system size at which oscillations start decreases with nutritional stress. We validate experimentally these two expectations, thereby supporting the hypothesis that stress oscillations in growing biofilms emerge through a delay-induced Hopf instability.

A DDE Model for Biofilm Stress Dynamics

We set out to build a dynamical model describing the behavior of the stress levels in the biofilm periphery, which we denote by $x(t)$. This variable is taken to represent the stress of the peripheral cells with respect to a baseline, such that it can take positive or negative values depending on whether stress levels are above or below this baseline. In its simplest form, we can assume that the dynamics of $x(t)$ are given by a production rate that depends on past stress levels, $f(x(t-\tau))$, and a linear degradation with rate δ:

$$\frac{dx}{dt} = f(x(t-\tau)) - \delta x. \qquad [1]$$

The time-delay parameter τ in Eq. **1** includes the time needed for the growth state of the periphery to affect the stress of the interior cells and the time that it takes for the stress signal coming from the interior to reach the peripheral cells (Fig. 2*A*).

To choose $f(x)$, we assume that peripheral cells always have some basal stress production C that is modified by the effect of the stress experienced by the periphery in the past (Fig. 2*A*). Up to a certain level, peripheral stress at a time τ ago, $x(t-\tau)$, would have halted growth and thus it would now, at time t, lead to a reduction in stress levels coming from the interior ($f(x) < C$). On the other hand, if stress was too high, the interior cells would have probably died, thus eliminating the feedback effect ($f(x) = C$). Conversely, past peripheral stress levels below baseline would have allowed growth at time $t-\tau$, leading to an increase in stress at time t ($f(x) > C$). Again, values of x well below the baseline would be indicative of no stress at all, and thus no feedback would be present ($f(x) = C$). A simple negative

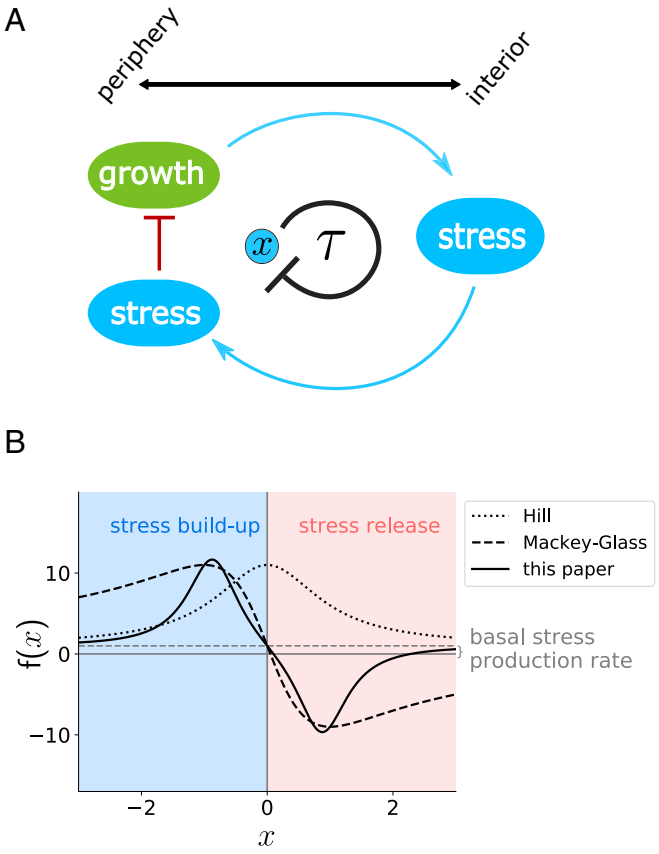

Fig. 2. A DDE model of biofilm oscillations. (*A*) Scheme of the model. Growth in the periphery leads to metabolic stress in the interior, which is transmitted to the periphery and inhibits growth. Therefore, stress in the periphery (x) is considered to exert a negative feedback on itself with some delay (τ). (*B*) Stress production function $f(x)$ for $C = 1$, $\alpha = 10$, $\beta = \gamma = 1$. The dashed gray line marks $f(x) = C$. The dotted black line is the Hill function $1 + \frac{10}{1+x^2}$. The dashed black line is the Mackey–Glass-like function $1 - \frac{20x}{1+x^2}$.

feedback expression like the Hill function $1/(1+x^2)$ (dotted line in Fig. 2*B*), which is often used to model self-inhibition (23, 24), is not appropriate here since it cannot change sign, and thus it would allow only for either stress release or buildup, irrespective of the amount of stress the biofilm had in the past. Another common representation of feedback is given by the classical Mackey–Glass function $(\alpha x)/(1+(x/\beta)^n)$ (19), originally proposed to model the production of mature blood cells. Subtracted to a basal production term C to agree with the explanation above, and in nondimensional form, would lead to the following expression for $f(x)$:

$$f(x) = C - \frac{\alpha x}{1+x^n}. \quad [2]$$

This function is plotted as a dashed line in Fig. 2*B*. Studies of the Mackey–Glass function have shown that it leads to supercritical Hopf bifurcations (25, 26), which are commonly found in dynamical systems including lasers (27), neurons (28), circadian clocks (29), and other biochemical circuits (30). Supercritical Hopf bifurcations arise when the fixed point of a system loses stability and a stable limit cycle appears, which overlaps in parameter space with the unstable steady state. The oscillation amplitude is zero at the bifurcation point and grows progressively as the system moves away from it (31). However, as stated previously, our biofilm oscillations start with nonzero amplitude. This is suggestive of a subcritical Hopf bifurcation, also commonly observed in natural systems (32–34). In this case, the limit cycle born at the bifurcation is unstable, overlapping in parameter space with the stable steady state. The unstable limit-cycle branch generally folds back into a stable limit cycle of nonzero amplitude, to which the system is attracted when the stable fixed point loses stability. Since this behavior is in better agreement with our observations, we searched for the simplest generalization of the model that would account for a subcritical Hopf bifurcation. We found that a quartic term in the denominator of $f(x)$, together with a negative squared term, leads to a subcritical bifurcation, as is shown in the following sections. Therefore, we consider the following form for $f(x)$ (solid line in Fig. 2*B*):

$$f(x) = C - \frac{\alpha x}{1-(x/\beta)^2+(x/\gamma)^4}. \quad [3]$$

The quartic term leads to faster loss of feedback with stress levels than a quadratic expression (compare the dashed and solid lines in Fig. 2*B* at the extreme x values). This is biologically realistic, since we expect biofilm viability and metabolic feedback to be lost quickly if stress becomes too high or too low, respectively. Additionally, the negative quadratic term leads to a weaker effect of stress on delayed stress production at low stress levels (compare the dashed and solid lines around $x=0$ in Fig. 2*B*). This is also biologically reasonable, since cells have a variety of homeostatic responses that enable them to maintain their physiological state under weak stress levels.

Delayed Negative Feedback Leads to Oscillations via a Hopf Bifurcation

To explore the behavior of the model, we begin by examining analytically how the delay term affects the dynamics of the system. Eqs. **1** and **3** has a steady-state solution, given implicitly by

$$C - \frac{\alpha\, x_s}{1-x_s^2+x_s^4} - \delta x_s = 0 \quad [4]$$

(we assume in what follows that $\beta=\gamma=1$). The stability of this stationary state is determined by introducing the ansatz $x(t) = x_s + \eta\exp(\lambda t)$ into Eqs. **1** and **3** and expanding $f(x)$ up to first order in η. This leads to the characteristic equation (35)

$$J_\tau \exp(-\lambda\tau) + J_0 - \lambda = 0, \quad [5]$$

where $\lambda \equiv \mu + i\nu$ is the complex eigenvalue of the steady-state solution, $J_0 = -\delta$ is the derivative of the right-hand side of Eqs. **1** and **3** with respect to the nondelayed variable $x(t)$, and J_τ is the derivative with respect to the delayed variable $x_\tau \equiv x(t-\tau)$, evaluated at the steady state:

$$J_\tau = -\frac{\alpha\, x_s\left(2x_s - 4x_s^3\right)}{(1-x_s^2+x_s^4)^2} - \frac{\alpha}{1-x_s^2+x_s^4}. \quad [6]$$

Expanded into its real and imaginary parts, the characteristic Eq. **5** takes the form

$$J_\tau \exp(-\mu\tau)\cos(\nu\tau) + J_0 - \mu = 0 \quad [7]$$

$$J_\tau \exp(-\mu\tau)\sin(\nu\tau) + \nu = 0. \quad [8]$$

A bifurcation in which the steady state given by Eq. **4** changes stability entails that μ goes through 0. Setting μ to 0 in Eqs. **7** and **8** leads to the following solution for ν:

$$\nu = \sqrt{J_\tau^2 - J_0^2}. \quad [9]$$

This solution exists provided $J_\tau^2 > J_0^2$. When this condition holds, a Hopf bifurcation arises in which the steady state changes stability while the imaginary part ν of the eigenvalue is nonzero. Such a bifurcation leads to an oscillatory, limit-cycle behavior with frequency ν at the bifurcation.

To make sense of the condition $J_\tau^2 > J_0^2$ given above, we now go to the limit of large δ (more explicitly, $\delta \gg C/\beta, C/\gamma$). This assumption is experimentally reasonable, since stress release in the biofilm can be expected to be fast, as it depends on the opening of ion channels (13) and on metabolic processes that operate on the order of minutes, whereas the period of the oscillations is on the order of hours. In this case $x_s \approx 0$. This can intuitively be seen by considering Eq. **4** as the crossing of the function $f(x)$ (Fig. 2*B*), which has a value of C at $x=0$, with the line $y=\delta x$, which has an increasingly higher slope as δ increases, and in the limit of a vertical line it would intersect the function at $x_s=0$. Since, according to Eq. **6**, $J_\tau = -\alpha$ for $x_s=0$, we can rewrite the condition for the existence of the Hopf bifurcation as $\alpha > \delta$. Therefore, for strong enough negative feedback the system exhibits a Hopf bifurcation leading to oscillations.

The Hopf Bifurcation Is Subcritical

To further characterize analytically the Hopf bifurcation exhibited by the system, we now rewrite Eqs. **1** and **3** as

$$\epsilon\frac{dx}{dt} = \widetilde{C} - \frac{\widetilde{\alpha}\, x(t-\tau)}{1-(x(t-\tau)/\beta)^2+(x(t-\tau)/\gamma)^4} - x, \quad [10]$$

where we define $\epsilon = \frac{1}{\delta}$, $\widetilde{C} = \frac{C}{\delta}$, and $\widetilde{\alpha} = \frac{\alpha}{\delta}$. Taking again the limit of large δ ($\epsilon \to 0$), the system reduces to the discrete map $x_{n+1} = \widetilde{f}(x_n)$ (36), where

$$\widetilde{f}(x) = \widetilde{C} - \frac{\widetilde{\alpha}x}{1-x^2+x^4}, \quad [11]$$

assuming again $\beta=\gamma=1$. In this discrete description, the condition for a Hopf bifurcation to occur at a critical value $\widetilde{\alpha}_c$ is (31)

$$\widetilde{f}_x\left(\widetilde{\alpha}_c, \widetilde{x}_s(\widetilde{\alpha}_c)\right) = -1, \quad [12]$$

where the subindex "x" in $\widetilde{f}_x$ indicates differentiation with respect to x, and $\widetilde{x}_s(\widetilde{\alpha}_c)$ denotes the steady state evaluated at $\widetilde{\alpha}_c$. Assuming without loss of generality that $\widetilde{C}=0$, the fixed point of the map such that $x_n = \widetilde{f}(x_n)$ is $\widetilde{x}_s = 0$, and $\widetilde{f}_x(\widetilde{\alpha}_c, \widetilde{x}_s) = -\widetilde{\alpha}_c$. This implies, according to Eq. **12**, that the critical value

of the rescaled feedback intensity is $\widetilde{\alpha}_c = 1$, corresponding to $\alpha_c = \delta$ and in agreement with the analysis made in the preceding section.

The stability of the steady state around the Hopf bifurcation point can be established by the quantity (37)

$$a = -\left(\widetilde{f}_{xx}\widetilde{f}_{\alpha} + 2\widetilde{f}_{x\alpha}\right), \qquad [13]$$

where the subindex "α" denotes differentiation with respect to $\widetilde{\alpha}$, and the partial derivatives are evaluated at the fixed point $\widetilde{x}_s$ and at the critical value $\widetilde{\alpha}_c$ of the control parameter. A linear stability analysis shows (37) that the steady state a small distance $\Lambda = \widetilde{\alpha} - \widetilde{\alpha}_c$ away from the bifurcation point is stable (unstable) if $a\Lambda < 0$ ($a\Lambda > 0$). Furthermore, the limit cycle emerging at the Hopf point corresponds in this discrete description to a period-2 fixed point $x_n = \widetilde{f}(\widetilde{f}(x_n))$, with $x_n = \widetilde{x}_s + \sqrt{-a\Lambda/b}$ (36) and b equal to

$$b = -\left(\frac{1}{2}\widetilde{f}_{xx}^{\,2} + \frac{\widetilde{f}_{xxx}}{3}\right). \qquad [14]$$

Considering again $\widetilde{C} = 0$, we find that a and b are both positive ($a = 2$ and $b = 2$). Therefore, the limit cycle that emerges at the Hopf bifurcation exists for $\Lambda < 0$ ($\widetilde{\alpha} < \widetilde{\alpha}_c$) and coexists with a stable fixed point (since $a\Lambda < 0$). We can thus conclude that the Hopf bifurcation exhibited by this system is subcritical. We note that the negative quadratic term in the denominator of Eq. **3** determines the subcritical nature of the bifurcation. If it is positive, then $a > 0$, $b < 0$, and the bifurcation becomes supercritical. If the quadratic term is not present, the parameter b becomes equal to 0, leading to a limiting behavior that would also be in disagreement with our experimental observations. We thus do not consider those two situations further.

Oscillations Can Coexist with a Stable Steady State

To determine whether the conclusion above holds for the complete system (with finite δ) we performed continuation analysis using the DDE-BIFTOOL software package (26). Fig. 3*A* shows that, as α increases, the system undergoes indeed a subcritical Hopf bifurcation (HB), from which an unstable limit-cycle branch emerges (whose extrema are represented by a dotted red line in Fig. 3*A*) that eventually folds back into a stable limit cycle (solid red line in Fig. 3*A*), in what is known as a fold bifurcation of limit cycles (FLC). Importantly, between the FLC and HB bifurcations the stable limit cycle coexists with the stable steady state, resulting in a region of bistability. Within that region, the oscillatory dynamics shown in Fig. 1 are expected to coexist with a nonoscillating state in which the biofilm grows in a monotonic manner. As a result of this bistability, a perturbation of the stable steady state (in the form, for instance, of a temporary increase in the basal stress production parameter C) should make the biofilm jump to the oscillatory attractor. This can be observed numerically in Fig. 3*B*, which shows the response of the stress variable x in our model to a brief perturbation (represented by the vertical gray region in the plot).

According to the bifurcation behavior described above, we should expect that perturbing experimentally an otherwise stationary biofilm should lead to oscillations when it is perturbed. To ease comparison with experiments, we model the dynamics of ThT as a reporter located downstream of x. To that end, we assume that ThT ($\mathcal{T}$) accumulates in the cell as x increases in a sigmoidal manner with threshold x_{th} and decays linearly (13):

$$\frac{d\mathcal{T}}{dt} = \frac{\alpha_{\mathcal{T}}}{\exp[(x_{\mathrm{th}} - x)/\sigma] + 1} - \delta_{\mathcal{T}}\,\mathcal{T}. \qquad [15]$$

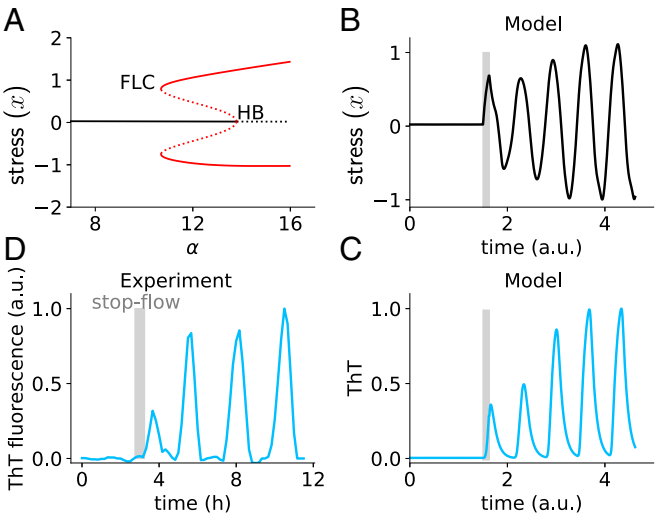

Fig. 3. The system has a subcritical HB. (*A*) Bifurcation diagram of the model with respect to α, for $C = 0.5$, $\tau = 0.25$, $\beta = \gamma = 1$, $\delta = 10$. The black lines represent steady states; the red lines denote limit cycles [with solid (dotted) corresponding to stability (unstability)]. HB, Hopf bifurcation; FLC, fold bifurcation of limit cycles. (*B* and *C*) Simulation for $\alpha = 12.5$. The gray region denotes a perturbation of parameter *C*, which is increased to 10 for 0.125 time units. The ThT trace is normalized to its maximum. ThT parameters: $\alpha_{\mathcal{T}} = 10$, $x_{\mathrm{th}} = 0.6$, $\sigma = 0.1$, $\delta_{\mathcal{T}} = 10$. (*D*) Experimental ThT time trace showing the response to a 30-min stopping of nutrient flow (gray region).

Fig. 3*C* shows the dynamics of ThT corresponding to the $x(t)$ time trace in Fig. 3*B*. The plot confirms that ThT responds in a bistable manner, remaining in a (stable) stationary solution until it is perturbed, at which point it jumps to the coexisting oscillatory attractor. We are now ready to validate this expectation in our experiments.

To perturb the biofilm experimentally we use the fact that, in our setup, nutrients (in particular glutamate) are flowing through the microfluidic device in a continuous manner. We can thus perturb the biofilm by stopping the flow temporarily, which leads to a sudden increase in glutamate starvation and stress and is thus analogous to increasing the C parameter in the model. We call this a "stop-flow" perturbation in what follows. Fig. 3*D* shows the response of the biofilm to such perturbation (again represented by a vertical gray bar). In agreement with the subcritical nature of the bifurcation exhibited by the model, transiently stopping the flow in growing biofilms triggers the emergence of oscillations, which quickly reach their final amplitude. We thus conclude that the stress oscillations exhibited by the biofilm coexist in a bistable manner with a nonoscillating state, as expected from the delay-differential model proposed above.

Oscillations Require a Minimum System Size

As biofilms grow their size increases, and therefore the parameter that drives the system to the bifurcation point should be the delay τ rather than α. Solving Eqs. **7** and **8** for τ with $\mu = 0$ leads to the exact critical value of the delay at which the bifurcation occurs,

$$\tau_c = \sqrt{\frac{\arccos(-J_0/J_\tau)^2}{J_\tau^2 - J_0^2}} = \sqrt{\frac{\arccos(\delta/J_\tau)^2}{J_\tau^2 - \delta^2}}, \qquad [16]$$

which, again, exists provided $J_\tau^2 > \delta^2$. Continuation analysis confirms that the system can also undergo a subcritical HB when increasing τ, as shown in Fig. 4*A*. Fig. 4*A* shows that there is also a large region of bistability in this case. Thus, the model predicts

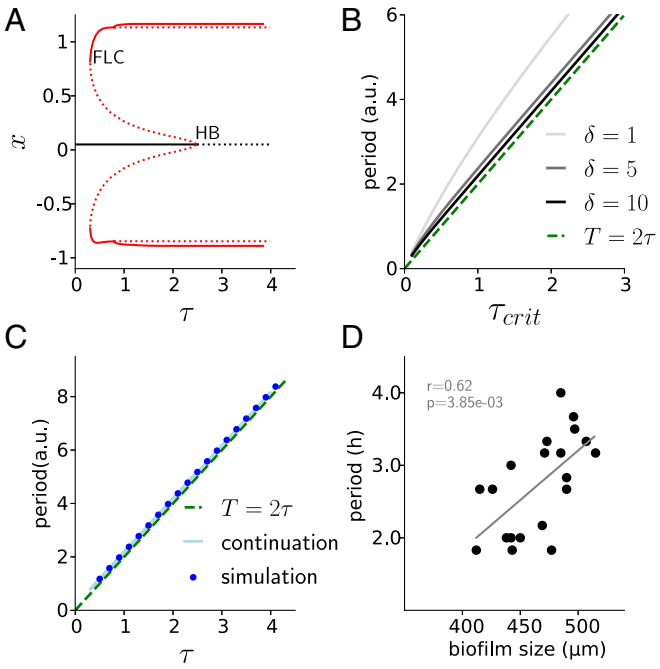

Fig. 4. The subcritical HB can be controlled by the time delay (τ). (*A*) Bifurcation diagram as a function of τ, for $C = 1$, $\alpha = 10$, $\beta = 1$, $\gamma = 1$, $\delta = 10$. (*B*) Analytic relationship between the oscillation period and the time delay for different values of δ (solid lines), according to Eq. **17**. The green dashed line shows the limit of infinite δ: $T = 2\tau$. (*C*) Numerical relationship between the oscillation period and the time delay for the same parameter values as in *A*. The light blue line is the result of continuation analysis with DDE-BIFTOOL, the blue solid circles show simulation results, and the green dashed line is the relationship $T = 2\tau$, for reference and comparison with *B*. (*D*) Period at the oscillation onset as a function of biofilm size (radius). Scatterplot, experimental data; gray line, linear fit; r, correlation coefficient; p, *P* value.

that for small delays the system is at a steady state, it then enters a bistable region, and it finally crosses the bifurcation point, where only an oscillatory steady state remains. Incidentally, period-doubling bifurcations arise when τ increases (branching of red line in Fig. 4*A*), and higher-order doublings arise for larger values of C. Since the relationship of these phenomena to the experimental data is unclear, we do not comment further on it.

We can also explore theoretically the relationship between the period of the oscillations and the time delay. To that end, we assume that the oscillation frequency will be given approximately by the imaginary part ν of the eigenvalue of the steady state, which is true at the bifurcation point. Combining Eqs. **7** and **8** through the elimination of $\exp(-\mu\tau)$ leads to the following equation for ν,

$$0 = \frac{-\nu}{\delta + \mu} - \tan(\nu\tau) \approx \frac{-\nu}{\delta} - \tan(\nu\tau), \qquad [17]$$

where we assume again the limit of large $\delta \gg \mu$. In that limit, the equation above has three solutions for $\nu\tau$ in $[-\pi, \pi]$, which are asymptotically close to 0, π, and $-\pi$. Taking into account that $J_\tau \approx -\alpha < 0$ for large δ and that $J_0 = -\delta < 0$ in any case, Eqs. **7** and **8** lead to the conclusion that $\cos(\nu\tau) < 0$ (and close to -1) and $\sin(\nu\tau) > 0$ (and close to 0). The only one of the three solutions listed above that fulfills these conditions is $\nu\tau \approx \pi$. Therefore, in the limit of large δ we can expect the oscillation period to be $T \sim 2\pi/\nu \approx 2\tau$. This expression is shown as a green dashed line in Fig. 4*B*. Fig. 4*B* also plots the result of numerically solving Eq. **17** for different finite values of δ. For $\delta = 10$, for instance, the relationship between the period and the critical delay lies slightly above the line $T = 2\tau$. Moreover, this relationship also holds for delay values away from the bifurcation point. This is shown in Fig. 4*C* for the parameter values of Fig. 4*A*. The light blue line plots the results of the continuation analysis, and the solid circles are the results of numerical simulations. This linear relationship between the period and the delay is consistent with the experimental observations (Fig. 4*D*), as well as with the previously reported increase of period over time in oscillating biofilms (extended data figure 1b in ref. 12), further validating our interpretation of the time delay as being directly related with the biofilm size.

The bifurcation behavior shown in Fig. 4*A* indicates that beyond a critical delay (corresponding to a critical biofilm size), the only stable attractor of the system is an oscillatory one. However, even before that critical size is reached, the biofilm can be induced to oscillate if properly perturbed (as shown in Fig. 3). The "ease" with which a perturbation will induce the biofilm to jump from steady to oscillatory growth within the bistable region is (roughly) inversely related to the size of the basin of attraction of the stable fixed point. An indication of the size of this basin of attraction is provided by the amplitude of the unstable limit cycle (dotted red line in Fig. 4*A*) surrounding the stable fixed point (solid black line in Fig. 4*A*). The bifurcation diagram shows that the unstable limit cycle gets closer to the stable fixed point as τ (and hence the system size) increases. Therefore, the model predicts that the closest the system is to the bifurcation point, the easiest it will be that a perturbation drives it out of the stable fixed point and into the oscillatory attractor. This agrees well with the experimental data shown in Fig. 5*A*, where larger biofilms

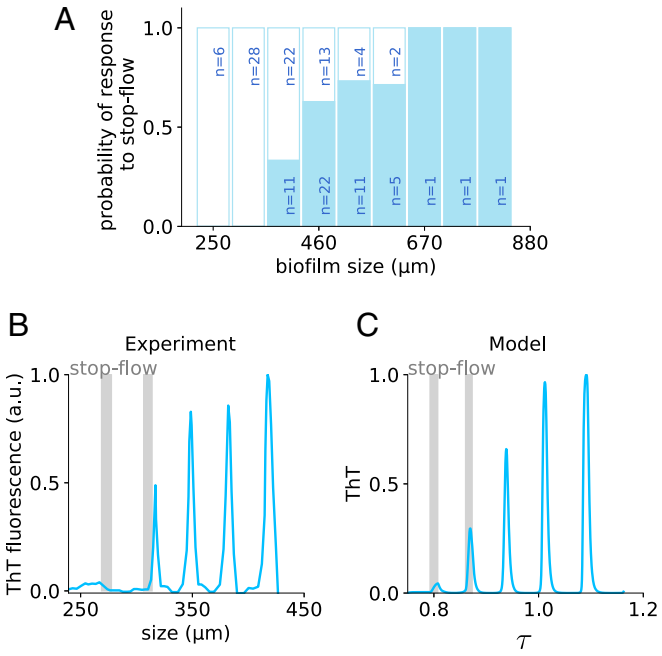

Fig. 5. Oscillation triggering in the bistable regime is easier for larger biofilms. (*A*) Fraction of experiments (solid blue bars) in which a stop-flow perturbation triggers oscillations in growing biofilms. The flow was stopped for 30 min and the appearance of oscillations was assessed. Nonresponding biofilms are indicated by the white bars. (*B*) Sample ThT experimental time trace where an early application of a stop-flow perturbation (vertical gray bar) does not trigger oscillations, but a subsequent one when the system is slightly larger does. (*C*) Simulation of the system with increasing τ. Two subsequent stop-flow–type perturbations (increase of C to 3.5) were applied, at times 1.25 and 3.25, for 0.5 time units. Parameter values are those of Fig. 4, plus $\eta = 0.035$, $\delta_\tau = 0.02$, $\alpha_T = 10$, $x_{th} = 0.6$, $\sigma = 0.1$, and $\delta_T = 10$. Initial conditions are $\tau_0 = 0.75$, $T_0 = 0$, and $x_0 = 0.05$. ThT time trace is normalized to its maximum.

are more likely to start oscillating upon a stop-flow perturbation. Furthermore, biofilms under a minimum size of around 400 μm never oscillate, and those beyond a maximum size of around 670 μm always oscillate.

Since the biofilm is continuously growing, the responsiveness to perturbations depends on time: Perturbing the biofilm when it is too small does not result in oscillations, whereas a subsequent perturbation does (Fig. 5*B*). To model this behavior and explore the interplay between growth and consecutive perturbations, we assume that the time delay in Eq. **1** increases at a rate that diminishes with x, since when the biofilm is stressed above (below) the basal level, its growth rate will decrease (increase), and so will its size, and correspondingly the delay:

$$\frac{d\tau}{dt} = \eta - \delta_\tau x \qquad [18]$$

(parameters η and δ_τ are chosen in such a way that $d\tau/dt$ is always positive). We used these dynamics to investigate the response to two consecutive perturbations in the model. According to the simulations, if the system is too small, a stop-flow perturbation may not perturb the system sufficiently to make it jump to the oscillatory attractor (Fig. 5*C*). But a subsequent perturbation when the delay is larger can, as in the experiments (compare Fig. 5 *B* and *C*).

The Critical Size for Oscillation Onset Is a Function of the Stress Level

As shown in Fig. 4*A*, the bistability region is bounded on the right by the critical delay at which the HB occurs and on the left by the point at which the unstable limit cycle becomes stable at the FLC. We performed a continuation analysis to explore how these two bifurcation points change as a function of the delay τ and the basal stress production C. Fig. 6*A* represents the resulting phase diagram, where the purely oscillatory region is bound by the HB line (thick black line, with solid representing supercriticality and dashed subcriticality), and the bistable region is delimited by the subcritical HB line and the FLC line (dotted black line). A 1D vertical cross-section of this phase diagram for fixed τ is shown in Fig. 6*B* as a bifurcation diagram with respect to C and confirms that the entire region below the subcritical HB is indeed bistable. The phase diagram depicted in Fig. 6*A* shows that the bistability region is wide. Moreover, the analysis indicates that for high enough values of C the HB as a function of τ becomes supercritical and bistability is lost. At this point, $f(x)$ is highly biased toward positive values, mostly contributing to stress increase. This suggests that bistability requires the system to relieve stress sufficiently below baseline levels.

Within the bistable region, Fig. 6*A* also predicts that for higher basal stress levels (higher C), the critical delay at which the Hopf bifurcation happens (dashed line) is reduced, while the position of the fold bifurcation remains unchanged (dotted line). We confirm this result by adding noise to the system and integrating numerically the corresponding stochastic DDE (*Materials and Methods*) for different C and delay values. We compute the response of the system to a temporary increase of the basal stress production rate C for 100 realizations of the noise and quantify the fraction of simulations in which the system switches from the stable fixed point to the limit cycle attractor. In agreement with the continuation analysis, we found that for higher basal stress levels the system is able to respond to the perturbation for smaller delays (Fig. 6*C*). We can validate this prediction experimentally by tuning the glutamate concentration of the medium, with lower concentrations being associated with higher values of C. Identifying the cumulative distribution of sizes at which biofilms are found to oscillate (either naturally or upon a stop-flow perturbation) with the propensity of the biofilm to switch to oscillations for a given size, we observe (Fig. 6*D*) a good qualitative agreement with the model: For higher stress levels (lower levels of glutamate) the critical size to respond to perturbations is reduced. The model predicts that the range of the bistable sizes is reduced as stress increases, which is also in agreement with the experimental data (compare, e.g., the ranges of the magenta and green lines in Fig. 6 *C* and *D*).

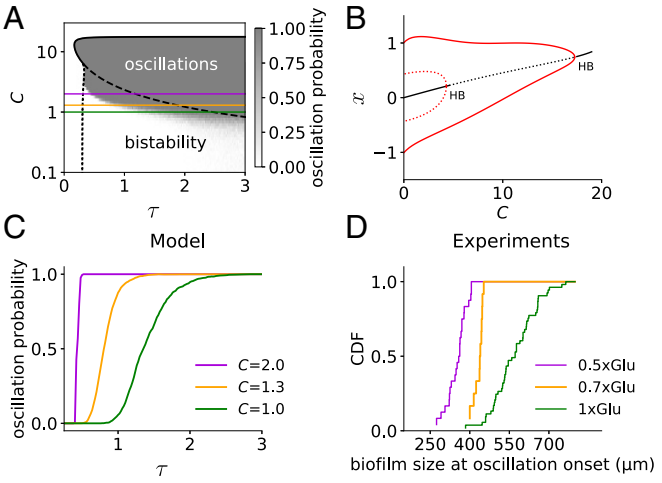

Fig. 6. Stress reduces the critical size for oscillations. (*A*) Phase diagram showing the position of the HB (solid and dashed black lines) and FLC (dotted black line), as a function of the basal stress production *C* and the feedback delay τ. The color map shows the probability of oscillation in stochastic simulations with stop flow consisting of an increase in *C* by a factor of 3 during 0.5 time units. Parameters are those of Fig. 4. (*B*) Bifurcation diagram as a function of *C* for fixed τ, corresponding to a vertical cross-section of *A* at $\tau = 0.5$. (*C*) Horizontal cross-sections of the gray field from *A* at different *C* levels (smoothed). (*D*) Experimental cumulative distribution functions (CDF) of the size at oscillation onset for three different glutamate concentrations.

Discussion

We have studied the transition to growth oscillations in bacterial biofilms. Our experiments show that the oscillations arise for a minimum biofilm size with finite amplitude. Here, we have proposed a minimal model to explain these features, assuming a general functional behavior of stress production. This simple mathematical model, in terms of a DDE, reveals the essential features of the transition to oscillations in this system. The model shows emergence of oscillations at a critical delay (which we link with biofilm size), through a subcritical HB. Such bifurcation entails the presence of a bistable regime in which the biofilms either oscillate in their growth or expand steadily, depending on the initial conditions. Experimentally, this expectation can be validated by temporarily stopping the media flow within the microfluidic device. Our experiments do show that such perturbations lead to oscillations in growing biofilms, provided they are large enough.

Biofilm oscillations were described to be a mechanism to prevent cells in the biofilm interior from dying due to starvation caused by the growth of peripheral cells, and this was shown to enable the regeneration of the community upon external chemical attacks (12). Therefore, the bistable behavior reported here could be a mechanism to allow oscillations to start early enough to ensure the survival of interior cells. Both the model and the data show that the critical size for biofilm oscillations depends on the nutrient concentration in the media. This is consistent with the fact that when nutrient levels are low, interior cells become starved earlier, thus triggering the emergence of the

oscillations at smaller sizes. Also, the discontinuous transition allows the biofilm to start oscillating immediately with a nonzero amplitude, instead of having to wait for the oscillations to slowly develop.

Our model is similar to the classical Mackey–Glass equation, which is well known to undergo period-doubling bifurcations that eventually lead to chaotic behavior (19, 25). We also observed such richness in dynamical behavior in our case. However, although mathematically interesting, we have not further analyzed it as it does not seem relevant to our experimental situation. In contrast, the good agreement between the model and the experimental data in terms of the discontinuous emergence of oscillations and the presence of bistability highlights the importance of developing simple mathematical models of biological systems, which allow us to establish the minimal conditions underlying specific biological phenomena.

Delayed feedback has been recognized as a source of dynamical behavior in many areas of science and engineering for years (35). Spatially structured biological populations provide a natural substrate for delayed interactions due to the finite propagation speed of biological signals. The results reported here show that such delayed interactions can have important collective effects in bacterial populations. It would be interesting to study the roles played by similar delay-induced mechanisms in other biological systems requiring global spatiotemporal coordination, such as developing organisms.

Materials and Methods

Biofilm Culture Conditions and Stop-Flow Procedure. *B. subtilis* biofilms were grown in microfluidics chips as described previously (12, 13). Media flow was driven by a pneumatic pump from the CellASIC ONIX Microfluidic Platform (EMD Millipore). The pump pressure was kept stable during the course of the experiments. We used a pump pressure of 1.5 psi with only one media inlet open, which maintains a media flow of 24 μm/s in the microfluidic chamber. During each stop-flow perturbation, the pump was turned off for 30 min. Biofilms were monitored using time-lapse microscopy, and we tracked metabolic oscillations within growing biofilms using 10 μM ThT. Experimental time traces are detrended using spline interpolation on the troughs of oscillations, smoothed and normalized to the maximum.

Continuation Analysis. Bifurcation diagrams were computed using the DDE-BIFTOOL v.3.1.1 package (26), run in Octave (38).

Simulations. Deterministic simulations of the system for fixed values of τ were carried out using the Python package pydelay v.0.1.1 (39). Deterministic simulations with state-dependent delays were performed using the routine ddesd (40) in Matlab (The MathWorks, Inc.). Initial conditions were the analytical steady state for the x variable and 0 for ThT.

To introduce noise into the system, we included an additive Gaussian white noise $\xi(t)$ in the stress equation,

$$\frac{dx}{dt} = C - \frac{\alpha\, x(t-\tau)}{1-(x(t-\tau)/\beta)^2+(x(t-\tau)/\gamma)^4} - \delta\, x + D\xi(t), \qquad [19]$$

with noise strength $D = 0.03$. We integrated this stochastic DDE with a custom-made code by adapting the stochastic Heun algorithm (41) to include the delay.

To calculate the oscillation probability at each combination of τ and C values (Fig. 6*A*), we performed 100 simulations per parameter combination. For each simulation, a random initial history array was generated from a uniform distribution in the interval $[0.5x_s, 1.5x_s]$, where x_s is the steady-state value. We then integrated Eq. **19** for 100 time units, at which point the C value was increased by a factor of 3 for 0.5 time units to simulate the stop flow and then returned to basal level for 1,000 time units. The last 100 time units were used to classify each trace as oscillatory or not, depending on whether it exhibited oscillations of amplitude larger than one.

ACKNOWLEDGMENTS. This work was supported by the Spanish Ministry of Economy and Competitiveness and Fondo Europeo de Desarrollo Regional (Project FIS2015-66503-C3-1-P) and by the Generalitat de Catalunya (Project 2017 SGR 1054). R.M.-C. acknowledges financial support from La Caixa Foundation. J.G.-O. acknowledges support from the Institució Catalana de Recerca i Estudis Avançats Academia programme and from the "María de Maeztu" Programme for Units of Excellence in Research and Development (Spanish Ministry of Economy and Competitiveness, MDM-2014-0370). J.L. acknowledges support from the J.L. acknowledges support from the Tsinghua–Peking Center for Life Sciences and the Thousand Talents Program of China. G.M.S. acknowledges support for this research from the San Diego Center for Systems Biology (NIH Grant P50 GM085764), the National Institute of General Medical Sciences (Grant R01 GM121888 to G.M.S.), the Defense Advanced Research Projects Agency (Grant HR0011-16-2-0035 to G.M.S.), and the Howard Hughes Medical Institute–Simons Foundation Faculty Scholars program (G.M.S.).

1. Winfree AT (2002) On emerging coherence. *Science* 298:2336–2337.
2. Zamora-Munt J, Masoller C, Garcia-Ojalvo J, Roy R (2010) Crowd synchrony and quorum sensing in delay-coupled lasers. *Phys Rev Lett* 105:264101.
3. Konigsberg IR (1971) Diffusion-mediated control of myoblast fusion. *Dev Biol* 26:133–152.
4. Aldridge J, Pye EK (1976) Cell density dependence of oscillatory metabolism. *Nature* 259:670–671.
5. Gregor T, Fujimoto K, Masaki N, Sawai S (2010) The onset of collective behavior in social amoebae. *Science* 328:1021–1025.
6. Hart Y, et al. (2014) Paradoxical signaling by a secreted molecule leads to homeostasis of cell levels. *Cell* 158:1022–1032.
7. Garcia-Ojalvo J, Elowitz MB, Strogatz SH (2004) Modeling a synthetic multicellular clock: Repressilators coupled by quorum sensing. *Proc Natl Acad Sci USA* 101:10955–10960.
8. Ng WL, Bassler BL (2009) Bacterial quorum-sensing network architectures. *Annu Rev Genet* 43:197–222.
9. Danino T, Mondragon-Palomino O, Tsimring L, Hasty J (2010) A synchronized quorum of genetic clocks. *Nature* 463:326–330.
10. De Monte S, d'Ovidio F, Danø S, Sørensen PG (2007) Dynamical quorum sensing: Population density encoded in cellular dynamics. *Proc Natl Acad Sci USA* 104:18377–18381.
11. Taylor AF, Tinsley MR, Wang F, Huang Z, Showalter K (2009) Dynamical quorum sensing and synchronization in large populations of chemical oscillators. *Science* 323:614–617.
12. Liu J, et al. (2015) Metabolic codependence gives rise to collective oscillations within biofilms. *Nature* 523:550–554.
13. Prindle A, et al. (2015) Ion channels enable electrical communication in bacterial communities. *Nature* 527:59–63.
14. Smolen P, Baxter DA, Byrne JH (2003) Reduced models of the circadian oscillators in *Neurospora crassa* and *Drosophila melanogaster* illustrate mechanistic similarities. *OMICS A J Integr Biol* 7:337–354.
15. Bratsun D, Volfson D, Tsimring LS, Hasty J (2005) Delay-induced stochastic oscillations in gene regulation. *Proc Natl Acad Sci USA* 102:14593–14598.
16. Novák B, Tyson JJ (2008) Design principles of biochemical oscillators. *Nat Rev Mol Cell Biol* 9:981–991.
17. Mather W, Bennett MR, Hasty J, Tsimring LS (2009) Delay-induced degrade-and-fire oscillations in small genetic circuits. *Phys Rev Lett* 102:068105.
18. Batzel JJ, Kappel F (2011) Time delay in physiological systems: Analyzing and modeling its impact. *Math Biosci* 234:61–74.
19. Mackey MC, Glass L (1977) Oscillation and chaos in physiological control systems. *Science* 197:287–289.
20. Lindner B, Doiron B, Longtin A (2005) Theory of oscillatory firing induced by spatially correlated noise and delayed inhibitory feedback. *Phys Rev E* 72:061919.
21. May RM (1973) Time-delay versus stability in population models with two and three trophic levels. *Ecology* 54:315–325.
22. Humphries J, et al. (2017) Species-independent attraction to biofilms through electrical signaling. *Cell* 168:200–209.
23. Lema MA, Golombek DA, Echave J (2000) Delay model of the circadian pacemaker. *J Theor Biol* 204:565–573.
24. Suzuki Y, Lu M, Ben-Jacob E, Onuchic J (2016) Periodic, quasi-periodic and chaotic dynamics in simple gene elements with time delays. *Sci Rep* 6:21037.
25. Wei J, Fan D (2007) Hopf bifurcation analysis in a Mackey–Glass system. *Int J Bifurcation Chaos* 17:2149–2157.
26. Engelborghs K, Luzyanina T, Roose D (2002) Numerical bifurcation analysis of delay differential equations using DDE-BIFTOOL. *ACM Trans Math Software* 28:1–21.
27. Ushakov O, et al. (2005) Coherence resonance near a Hopf bifurcation. *Phys Rev Lett* 95:123903.
28. Erchova I, Kreck G, Heinemann U, Herz A (2004) Dynamics of rat entorhinal cortex layer II and III cells: Characteristics of membrane potential resonance at rest predict oscillation properties near threshold. *J Physiol* 560:89–110.
29. van Zon JS, Lubensky DK, Altena PR, ten Wolde PR (2007) An allosteric model of circadian kaic phosphorylation. *Proc Natl Acad Sci USA* 104:7420–7425.
30. Goldbeter A (1996) *Biochemical Oscillations and Cellular Rhythms: The Molecular Bases of Periodic and Chaotic Behaviour* (Cambridge Univ Press, Cambridge, UK).
31. Strogatz SH (2014) *Nonlinear Dynamics and Chaos: With Applications to Physics, Biology, Chemistry, and Engineering* (Westview Press, Boulder, CO).
32. Resch P, Münster A, Schneider F (1991) A subcritical Hopf bifurcation in the methylene blue oscillator: Effects of imposed fluctuations. *J Phys Chem* 95:6270–6275.
33. Holzner R, Derighetti B, Ravani M, Brun E (1987) Observation of a subcritical Hopf bifurcation in a laser with an injected signal. *Phys Rev A* 36:1280–1287.

34. Del Negro CA, Hsiao CF, Chandler SH, Garfinkel A (1998) Evidence for a novel bursting mechanism in rodent trigeminal neurons. *Biophys J* 75:174–182.
35. Erneux T (2009) *Applied Delay Differential Equations* (Springer, New York).
36. Larger L, Goedgebuer JP, Erneux T (2004) Subcritical Hopf bifurcation in dynamical systems described by a scalar nonlinear delay differential equation. *Phys Rev E* 69:036210.
37. Larger L, Lee MW, Goedgebuer JP, Elflein W, Erneux T (2001) Chaos in coherence modulation: Bifurcations of an oscillator generating optical delay fluctuations. *JOSA B* 18:1063–1068.
38. Eaton JW, Bateman D, Hauberg S, Wehbring R (2015) *GNU Octave Version 4.0.0 Manual: A High-Level Interactive Language for Numerical Computations*. Available at https://octave.org/doc/interpreter/. Accessed August 9, 2018.
39. Flunkert V, Schöll E (2009) Pydelay – a python tool for solving delay differential equations. arXiv:0911.1633 [nlin.CD].
40. Shampine L (2005) Solving ODEs and DDEs with residual control. *Appl Numer Math* 52:113–127.
41. Toral R, Colet P (2014) *Stochastic Numerical Methods: An Introduction for Students and Scientists* (Wiley, Weinheim, Germany).